Assessment of the subgrid-scale models at low and high Reynolds numbers

By K. Horiuti[1]

1. Motivation and objectives

Large-eddy simulation (LES) is a turbulence simulation method in which the large scale (grid-scale or GS) field is directly calculated, while the small scale (subgrid-scale or SGS) field is modeled. The velocity and pressure fields (f) are decomposed into GS component ($\overline{f}$) and SGS component ($f' = f - \overline{f}$) using a filtering procedure. A decomposition of the SGS stress tensor, τ_{ij}, which results from filtering the Navier-Stokes equations, consists of three terms (Bardina 1983):

$$\tau_{ij} = L_{ij} + C_{ij} + R_{ij}, \tag{1}$$

$$L_{ij} = \overline{\overline{u}_i \overline{u}_j} - \overline{u}_i \overline{u}_j, \qquad C_{ij} = \overline{\overline{u}_i u'_j + u'_i \overline{u}_j}, \qquad R_{ij} = \overline{u'_i u'_j}.$$

L_{ij} is the Leonard term, C_{ij} is the cross term, and R_{ij} is the SGS Reynolds stress. The indices $i = 1, 2$, and 3 correspond to the directions x, y, and z, respectively, where x is the streamwise direction, y is the wall-normal or cross-stream direction, and z is the spanwise direction. In the present study, we consider fields which are homogeneous in two directions (x and z). We apply the Gaussian filter in the homogeneous directions because scale-similarity models are used to approximate the SGS stress tensors. No filter was applied in the inhomogeneous direction, but the same numerical discretization method was used in the y-direction in both the direct numerical simulation (DNS) data generation and assessing the LES models. In the following, $\langle\rangle$ denotes the average in the $x - z$ plane.

Our investigation is mostly focused on the SGS Reynolds stress R_{ij}. The SGS models commonly used for LES to represent the effects of the SGS on the GS are divided into two groups; SGS eddy viscosity coefficient models (EVM) and scale-similarity models.

Accurate SGS models must be capable of correctly representing the energy transfer between GS and SGS. Recent direct assessment of the energy transfer carried out using direct numerical simulation (DNS) data for wall-bounded flows (Piomelli *et al.* 1990, 1991) revealed that the energy exchange is not unidirectional. Although GS kinetic energy is transferred to the SGS (forward scatter (F-scatter) on average, SGS energy is also transferred to the GS. The latter energy exchange (backward scatter (B-scatter) is very significant, i.e., the local energy exchange can be backward nearly as often as forward and the local rate of B-scatter is considerably higher than the net rate of energy dissipation (Piomelli *et al.* 1991). Moreover, a mean

1 Department of Mechano-Aerospace Engineering, Tokyo Institute of Technology

reverse flow of energy from SGS to GS fluctuating turbulent motions was observed in the buffer layer region of the channel (Horiuti 1989, Härtel *et al.*1994). In free shear flows, a greater degree of B-scatter was observed in the mixing layer (Horiuti 1997)

EVM relates the SGS stress to the GS velocity deformation via the eddy viscosity. All SGS EVMs are derived from the Smagorinsky model (Smagorinsky 1963). In general, an EVM is adequate for approximating the interaction between given turbulent scales and distinctly smaller scales, in which the main function of the SGS is to remove energy from the GS, but it is inadequate for representing the B-scatter. A dynamic Smagorinsky model (Germano *et al.* 1991) can be used to model partial B-scatter in regions of reduced eddy viscosity, but strong B-scatter would require a negative eddy viscosity, which would lead to numerically unstable solutions, although a recent dynamic localization model (Ghosal *et al.* 1995a) may avoid this instability.

An alternative SGS model for EVM is the scale-similarity model (Bardina 1983). A representative model is the Bardina model in which the SGS Reynolds stress term is approximated as (Bardina 1983, Horiuti 1993a):

$$R_{ij} \simeq R_{ij}^B = C_B(\overline{u}_i - \overline{\overline{u}}_i)(\overline{u}_j - \overline{\overline{u}}_j). \tag{2}$$

Note that the model constant C_B cannot be determined using only the Galilean invariance constraint (Speziale 1985), but needs to be optimized (Horiuti 1993a, 1994, 1997). We have optimized C_B using several DNS data for incompressible channel and mixing layer flows so that the root-mean-square (rms) value of the modeled SGS Reynolds stress term approaches its value based on DNS data. Representative optimized values of C_B were in the range between 2.0 and 9.0 (Horiuti 1993a, 1993b, 1997).

The Bardina model for the SGS Reynolds stress (Eq. 2) gave better agreement between the exact and modeled SGS Reynolds stresses than the Smagorinsky model (Bardina 1983, Horiuti 1989, 1993a). This model, in which the SGS stress is no longer aligned with the GS strain rate, can exhibit B-scatter (Horiuti 1989, 1997).

The drawback inherent in the Bardina model, however, is that the predicted magnitude of the B-scatter contribution is larger than the exact DNS value. To overcome this problem, the filtered Bardina (F-Bardina) model

$$R_{ij} \simeq C_B\overline{(\overline{u}_i - \overline{\overline{u}}_i)(\overline{u}_j - \overline{\overline{u}}_j)}, \tag{3}$$

was proposed (Horiuti 1997). This model was obtained by utilizing the elliptic relaxation model procedure (Durbin 1993) to incorporate the nonlocal effect in physical space into the Bardina model. A marked improvement was obtained using the F-Bardina model compared with the Bardina model. The SGS Reynolds stress tensor approximated using the F-Bardina model was much closer to the exact DNS value than that obtained using the Bardina model. Also, the overestimation of the B-scatter obtained using the Bardina model was significantly reduced when the F-Bardina model was used.

High Re		
(i,j)	Bardina	F-Bardina
(1,1)	0.63	0.81
(1,2)	0.55	0.71
(2,2)	0.53	0.71
(3,3)	0.56	0.74

TABLE I: Correlation coefficients between the exact SGS Reynolds stresses and the those obtained using the different models for the high Reynolds number channel flow.

The testing of Horiuti (1997), however, was conducted using DNS data from a low Reynolds number channel and mixing layer flows. It was felt that further testing at higher Reynolds numbers was a necessary step needed to establish the validity of the new model. This is the primary motivation of the present study. The objective is to test the new model using DNS databases of high Reynolds number, fully developed turbulent channel and mixing layer flows.

2. Accomplishments

In the present study, we make use of direct numerical simulation flow fields available at CTR to directly test the various approximations. To compute the large-eddy flow fields, we filter the DNS fields by applying a two-dimensional Gaussian filter in the $i = 1$-,3-directions.

The high Reynolds number DNS databases were for the fully developed incompressible channel and the time-developing mixing layer flows. The channel flow DNS data was generated at $Re_\tau = 590$ (Reynolds number based on the wall-friction velocity, u_τ, and the half-channel height, δ) using $384 \times 257 \times 384$ grid points in the x-$\times y$-$\times z$-directions (Mansour 1996). The incompressible mixing layer DNS data was at $Re_\theta = 2400$ (the Reynolds number based on the momentum thickness, δ_m, and the velocity difference, ΔU) using $512 \times 180 \times 192$ grid points in the x-$\times y$-$\times z$-directions (TBL case; Rogers & Moser 1994). The results are compared with the previous assessment for low Reynolds numbers ($Re_\tau = 180$ for channel flow, and $Re_\theta = 200$ for mixing layer, Horiuti 1997).

2.1 Model assessment for channel flow

The high Reynolds number channel flow field was filtered to $64 \times 257 \times 64$ grid points in the x-, y-, and z-directions, respectively. The low Reynolds number channel flow field (with $128 \times 129 \times 128$ grid points) was filtered to $32 \times 129 \times 32$ grid points. These numbers of LES grid points were chosen so that the turbulent kinetic energy retained in the SGS components is large. This is necessary to make a fair assessment of the SGS models.

Table I lists the correlation coefficients between the exact SGS Reynolds stress tensor and those obtained using the Bardina and F-Bardina models for the high Re_τ case. For comparison, the previous results obtained for the low Reynolds number are

Low Re		
(i,j)	Bardina	F-Bardina
(1,1)	0.71	0.86
(1,2)	0.66	0.77
(2,2)	0.64	0.81
(3,3)	0.65	0.81

TABLE II: Correlation coefficients between the exact SGS Reynolds stresses and the those obtained using the different models for the low Reynolds number channel flow.

listed in Table II. The results obtained using the F-Bardina model are remarkably improved compared with those obtained using the Bardina model.

The GS and SGS fields interact via the SGS production term P due to the SGS Reynolds stress R_{ij}, i.e., $P = -\overline{u_i' u_j'}(\partial \overline{u}_i/\partial x_j + \partial \overline{u}_j/\partial x_i)/2$. The accuracy of the models is assessed by considering the prediction of the GS-SGS energy transfer. Figure 1 shows the y-distribution of the fraction of grid points in each $x-z$ plane where the B-scatter occurs in the P term. The optimized C_B values for the Bardina and F-Bardina models were, respectively, 3.5 and 4.3 for the low Re_τ case. For the high Re_τ case, the $C_B$value was approximately 9.0 for both models. In Fig. 1, R_{ij} is estimated from the exact SGS Reynolds stress. The results obtained by using the Bardina and F-Bardina models for the R_{ij} term are also included.

Approximately 30% of the grid points experience the B-scatter in the region $y_+ > 50$ for the low Re_τ case, but the fraction for the high Re_τ case is generally smaller than that for the low Re_τ case. A sharp decrease occurs at $y_+ \approx 10$, where the maximum (net) SGS production ($\langle P \rangle$) is the largest, for both Re_τ. This decrease is more considerable for the high Re_τ case. This decrease was not discernible in the results of Piomelli *et al.* (1991) in which a spectral cutoff filter was used instead of the Gaussian filter. Leslie and Quarini (1979) analytically found that when the Gaussian filter is used, the B-scatter contribution to the wave-number-dependent eddy viscosity is greatly reduced compared with that of the cutoff filter, which is consistent with the present results.

Throughout the channel, the fraction predicted using the Bardina model is much larger than the DNS exact value for both Reynolds numbers. Marked improvement is obtained by using the F-Bardina model.

The production term P is decomposed into the forward scatter part (defined as $(P + |P|)/2$, denoted by P_+) and the backward scatter part ($(P - |P|)/2$, denoted by P_-). In Fig. 2, we compare the y-distributions of the plane-averaged P_+ and P_- values obtained using the models with the exact values obtained from the DNS data for the low Re_τ case. The Bardina model overestimates the B-scatter term, whereas the results obtained using the F-Bardina model are in good agreement with the exact DNS data. These results are consistent with those observed in the fraction profiles shown in Fig. 1.

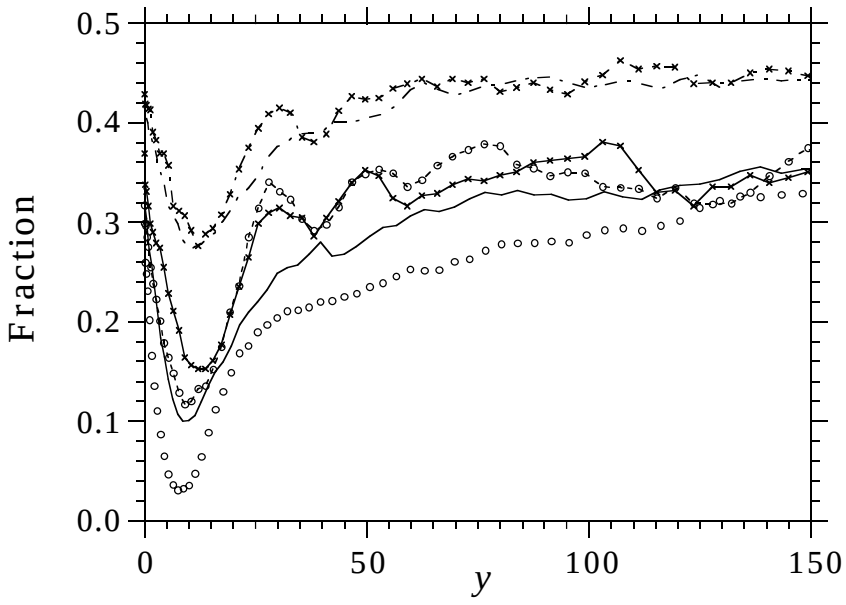

FIGURE 1. y-profiles of the fraction of grid points in each $x-z$ plane where the SGS production term, $P<0$ from channel flow. $\cdots\circ\cdots$, Exact (low); —-×—- , Bardina (low); -- × --, F-Bardina (low); ∘ , Exact (high); —-— , Bardina (high); ——— , F-Bardina (high).

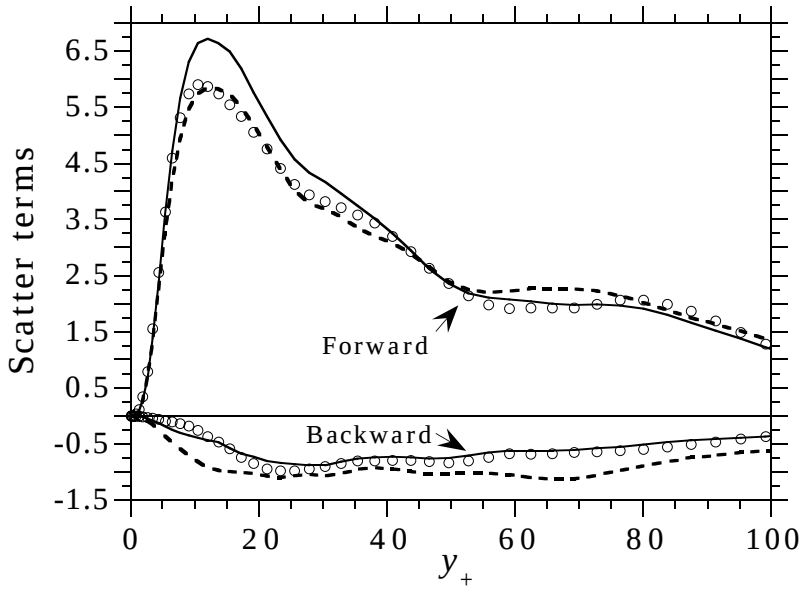

FIGURE 2. Decomposition of the plane-averaged SGS production term P obtained from the DNS exact data and obtained using different models from low Re_τ channel flow. Symbols: ∘ , Exact; ---- , Bardina; ——— , F-Bardina.

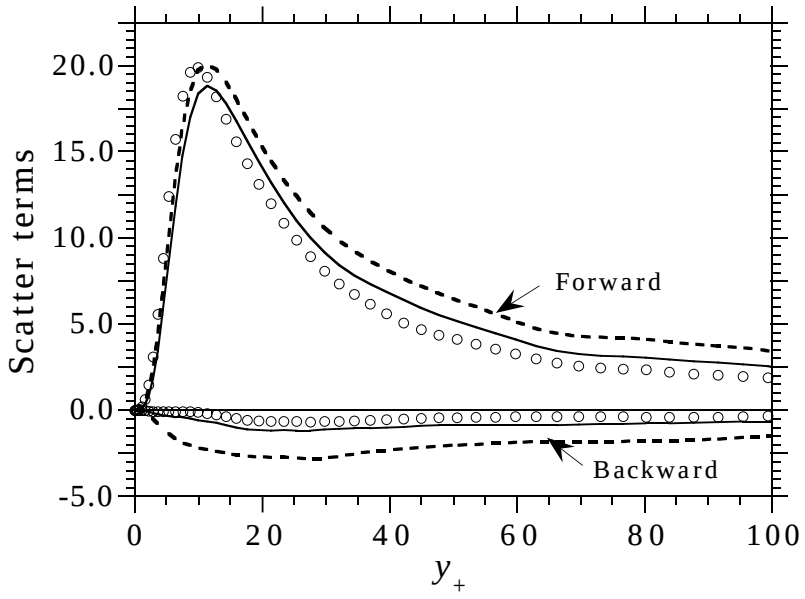

FIGURE 3. Decomposition of the plane-averaged SGS production term P obtained from the DNS exact data and obtained using different models from high Re_τ channel flow. Symbols as in Fig. 2.

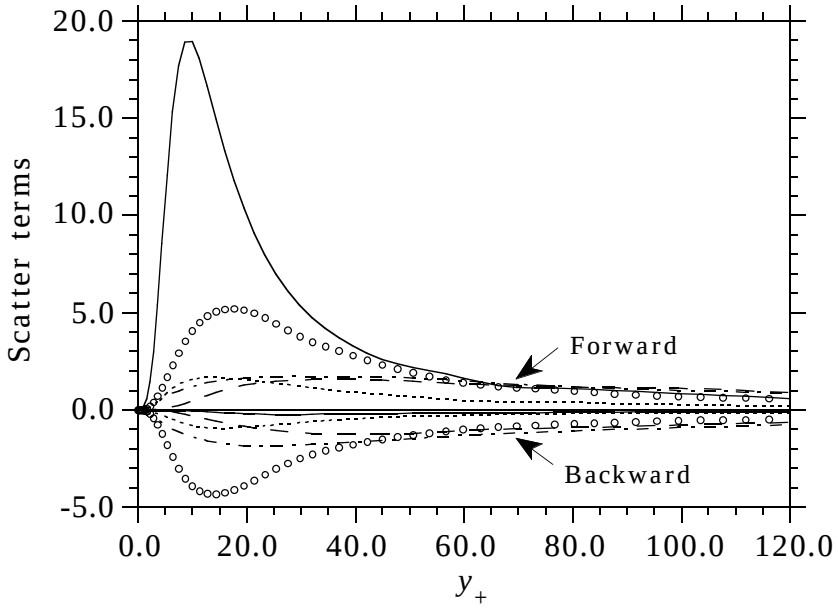

FIGURE 4. Decomposition of the plane-averaged P_{ij} terms obtained from DNS of high Re_τ channel flow. Symbols: ○ , (1,1); ——— , (1,2); ····· , (1,3); - - - - , (2,2); —·— , (3,3).

The corresponding result for the high Re_τ case is shown in Fig. 3. The exact values show that the energy transfer is predominantly forward near the wall as was found in Fig. 1. An overestimate of the B-scatter term for the Bardina model is more pronounced than in the low Re_τ case, whereas the F-Bardina model does not yield the excessive prediction of the B-scatter observed in the Bardina model. The F-Bardina model gives a sufficient GS energy drain when C_B is properly chosen, with an accurate prediction of the B-scatter being yielded concurrently (Horiuti 1997) for both Reynolds numbers, which implies that this model may be used as an alternative to the SGS EVM.

To determine the local rate of SGS production, we have examined the root-mean-square (rms) value of P (figure not shown). It was found that the local variance of P was two to six times larger than the plane-averaged value as was pointed out in Piomelli (1991).

Figure 4 shows the plane-averaged profiles of the individual components of the SGS production term $P_{ij} = -(\overline{u'_i u'_k}\partial\overline{u}_j/\partial x_k + \overline{u'_j u'_k}\partial\overline{u}_j/\partial x_k)$, in which R_{ij} is estimated from the exact SGS Reynolds stress of the high Re_τ channel flow. These terms are decomposed into two-parts that contribute to F- ($P_{ij} > 0$) and B- ($P_{ij} < 0$) scatters. It is found that the shear production term, P_{12}, is dominant in the region at $y_+ \approx 10$. The energy transfer arising in this term is predominantly forward due to the presence of the large mean shear rate near the wall. Away from the wall, however, the P_{12} term becomes gradually small and instead the normal production term, particularly the P_{11} term, becomes dominant. It can be seen that the magnitudes of the F- and B- scatter terms in P_{11} are very close to each other, with the total sum of P_{11} being slightly positive, but the sum becomes negative in the region at $y_+ \approx 15$. Correlations of the occurrence of this B-scatter event with the coherent vortical structure, which is oriented perpendicular to the wall, are discussed in Horiuti (1995).

An almost equal occurrence of F- and B- scatter is found similarly in other components. We note that the individual components, P_{ij}, were better approximated by using the F-Bardina model than by the Bardina model (figure not shown). Additionally, we found that the transfer between SGS and the fluctuating GS was predominantly backward as was previously pointed out by Horiuti (1997, figure not shown). Similar results were obtained for the low Re_τ channel flow.

2.2 Model assessment for mixing layer

The high Reynolds number mixing layer field was filtered to $128 \times 180 \times 48$ grid points in the x-, y- and z-directions. The low Reynolds number mixing layer flow field (with $192 \times 129 \times 128$ grid points) was filtered to $96 \times 129 \times 64$ grid points.

Table III lists the correlation coefficients between the exact SGS Reynolds stress tensor and those obtained using the Bardina and F-Bardina models for the high Re_θ case. Table IV lists the results for the low Reynolds number case. As in the channel flow, the results obtained using the F-Bardina model are significantly improved compared with those obtained using the Bardina model. We note, however, that the values of the correlation coefficients are generally lower for the high Reynolds number case than for the low Reynolds number case in both flows.

High Re		
(i,j)	Bardina	F-Bardina
(1,1)	0.66	0.82
(1,2)	0.55	0.68
(2,2)	0.63	0.81
(3,3)	0.63	0.80

TABLE III: Correlation coefficients between the exact SGS Reynolds stresses and the those obtained using the different models for the high Reynolds number mixing layer.

Low Re		
(i,j)	Bardina	F-Bardina
(1,1)	0.87	0.93
(1,2)	0.85	0.92
(2,2)	0.87	0.94
(3,3)	0.88	0.94

TABLE IV: Correlation coefficients between the exact SGS Reynolds stresses and the those obtained using the different models for the low Reynolds number mixing layer.

The optimized C_B values in the Bardina and F-Bardina models were 5.0 and 7.0, respectively, for the high Re_θ case. For the low Re_θ case, the optimized C_B values in the Bardina and F-Bardina models were 2.0 and 2.5, respectively. All of the optimized C_B values are between 2.0 and 9.0, and are rather independent of the type of flow.

Figure 5 shows the fraction of grid points at which the B-scatter occurs in P estimated from the exact SGS Reynolds stress for low and high Reynolds numbers. For the low Re_θ case, the fraction is over 40% throughout the vortical region of the mixing layer, and is generally larger than in the low Reynolds number channel flow (Fig. 1). The fraction, however, is significantly decreased for the high Re_θ case (approximately 30% throughout the vortical region). The fraction profiles implied by the Bardina and F-Bardina models for the R_{ij} term in P are also included in Fig. 5. The overestimate of the fraction in the results obtained using the Bardina model is more pronounced for the high Re_θ case than for the low Re_θ case.

Plane-averaged F- and B-scatter term values are shown in Figs. 6 and 7, respectively, for the low and high Re_θ cases. It can be seen that the magnitudes of these two terms are very close to each other for the low Re_θ case, indicating that F- and B-scatters occur almost evenly, with the total sum of P being slightly positive. For the high Re_θ case, the magnitude of the B-scatter contribution is decreased. This is consistent with the fraction profiles shown in Fig. 5.

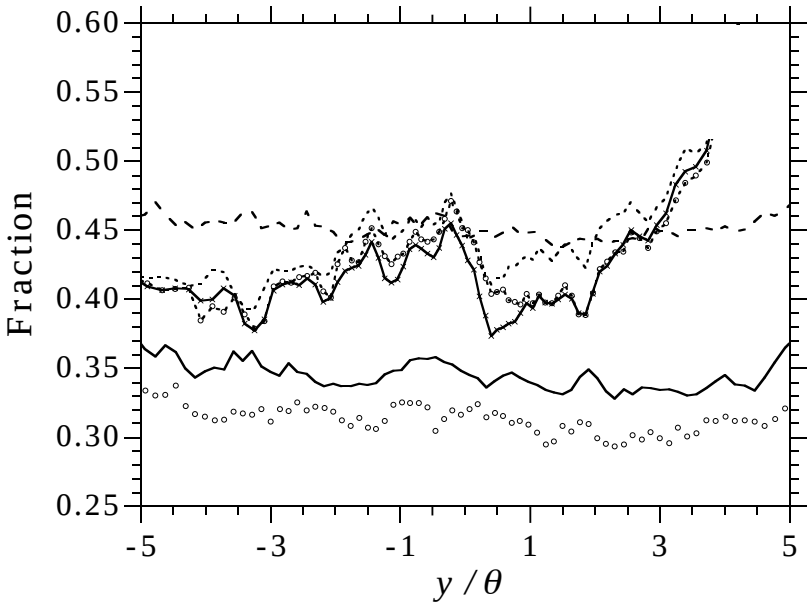

FIGURE 5. y-profiles of the fraction of grid points in each $x-z$ plane where the SGS production term $P < 0$ from mixing layer. $\cdots\circ\cdots$, Exact (low); ····· , Bardina (low); $--\times--$, F-Bardina (low); $\circ$, Exact (high); ---- , Bardina (high); ——— , F-Bardina (high).

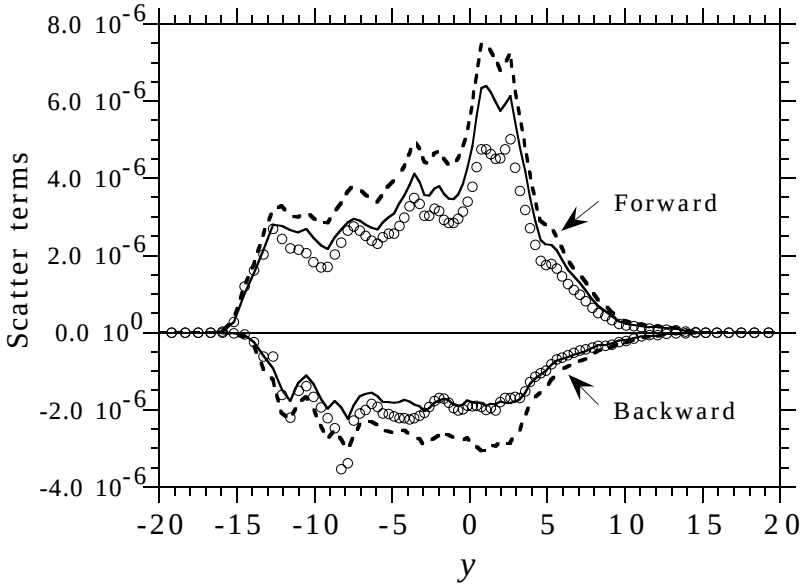

FIGURE 6. Decomposition of the plane-averaged SGS production term P obtained from the DNS exact data and obtained using different models from low Re_τ channel flow. Symbols as in Fig. 2.

In the spatial distributions of P that were estimated from the low Re_θ DNS data, it was found that a large SGS energy production occurs in the braid region of the mixing layer. At the time which the test was conducted, the roll-up of the Kelvin-Helmholtz (K-H) vortices was complete, and these two eddies started to merge. The predominantly streamwise vortices ("rib" vortices) resided in the braid region between the K-H rollers (Rogers & Moser 1994). The distribution of the production term was characterized by a very intermittent appearance of the strong F- and B-scatter regions that took place side by side with a quadruple-like structure (Horiuti 1997).

This quadruple structure was highly aligned with the rib vortices. The vorticity distribution in the cross section of the rib vortices was not exactly circular, but rather elliptic. The F-scatter event occurred in the 1st and 3rd quadrants of the rib vortices, and B-scatter was generated in the 2nd and 4th quadrants of the rib vortices. We consider that the presence of these rib vortices is the primary cause of the almost equal occurrence of F- and B- scatters in the low Re_θ mixing layer. The present results indicate that the B-scatter events may occur in a deterministic manner rather than in a stochastic manner.

The major axis of the elliptic vortex, the circulation of which was counterclockwise, was making a positive angle with the cross-stream (y) axis. As a result, the area of 1st and 3rd quadrants was larger than that of the 2nd and 4th quadrants. Subsequently, the magnitude of F-scatter was larger than the B-scatter. Similarly, in the clockwise elliptic vortices, their major axis was making a negative angle with the y axis, the resultant net-scatter was also forward.

This finding may be a result of the low Reynolds number of the DNS. The distributions of the SGS production term P for the high Re_θ case also exhibited the quadruple-like structure, but the four quadrants were not as distinctive as for the low Re_θ case, i.e., the 1st and 3rd quadrants of the F-scatter regions were dominant, taking over the 2nd and 4th quadrants.

Figure 8 shows the plane-averaged profiles of the individual components of the SGS production term P_{ij}, in which R_{ij} is estimated from the exact SGS Reynolds stress from the high Re_θ mixing layer. These terms are decomposed into the F- and B- scatter contributions.

In the low Re_θ case, the quadruple structure of the SGS production term distribution primarily arose in the P_{22} term. In the high Re_θ case, it can be seen that large contributions result from the normal production terms, P_{22} and P_{33}, but it was found that the correlation coefficient between the P_{22} term and the P_{33} term was negative, thus they almost canceled each other out. Although, unlike the channel flow (Fig. 4), the magnitude of the shear stress production terms of P_{23} and P_{12} is smaller than the normal production terms, F-scatter contributions are larger than the B-scatter contributions in the P_{23} and P_{12} terms. As a result, the total summation of the production term P became predominantly forward.

Although the four quadrants of the quadruple-like structure in the total production term P distribution for the high Re_θ case were not distinctive as in the low Re_θ case, the distributions of the P_{22} and P_{33} terms exhibited distinctive quadruple-like

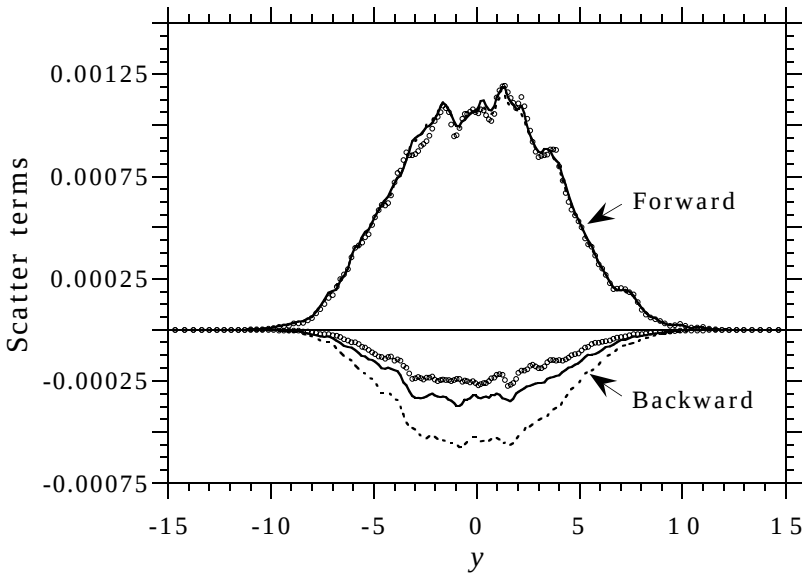

FIGURE 7. Decomposition of the plane-averaged SGS production term P obtained from the DNS exact data and obtained using different models from high Re_τ mixing layer. Symbols as in Fig. 2.

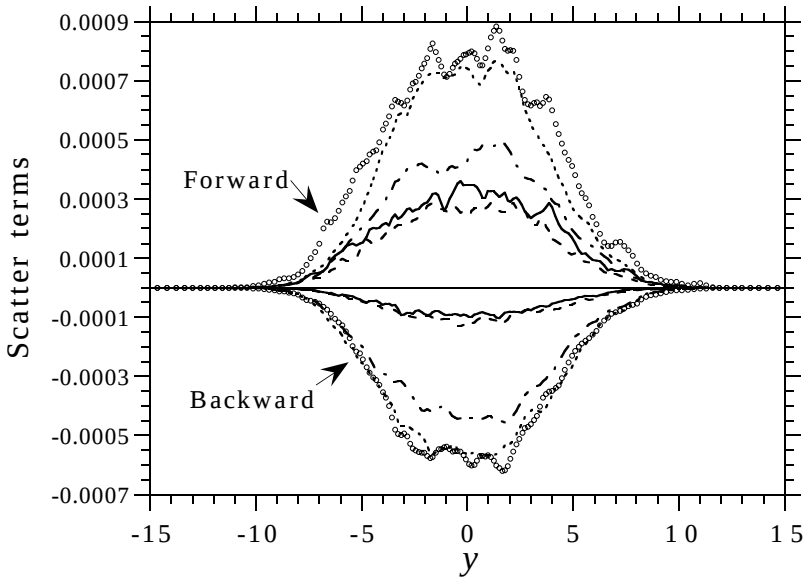

FIGURE 8. Decomposition of the plane-averaged P_{ij} terms obtained from the DNS exact data from high Re_τ mixing layer. —·— , (1,1); ——— , (1,2); ∘ , (2,2); - - - - , (2,3); ····· , (3,3).

structures. This fact indicates that the rib vortices resides in the high Reynolds number mixing layer on average as in the low Reynolds number and that the generation of a large SGS energy production occurs along the rib vortices. A negative correlation of the P_{22} term and the P_{33} term, however, was not depicted in the low Re_θ case.

3. Future plans

We have assessed the SGS models from the point of view of energy transfer between the grid scale (GS) and the subgrid-scale (SGS) via a correlation with the filtered DNS data ('a priori' test).

The energy transfer was directly analyzed using DNS data for fully developed turbulent channel and mixing layer flows for both high and low Reynolds numbers. A significant reduction of the B-scatter effect was found for the high Reynolds number case compared with the low Reynolds number case. We note, however, that the occurrence of F- and B-scatters may depend on grid resolution. For example, the rib vortices formed in the low Reynolds number mixing layer were only coarsely resolved (approximately 6 grid points for a single rib vortex), thus the SGS was significantly affected by the large GS motions. When the rib vortices are more finely resolved, the contributions of the B-scatter will decrease.

A capability of the scale-similarity models for the SGS Reynolds stress to represent the transfer was further tested. It was shown that the Bardina model is, in general, an inaccurate model for the SGS Reynolds stress. Its inaccuracy was greater for the high Reynolds number case for both flows. In a new scale-similarity model (filtered-Bardina, F-Bardina, model), the correlation with the DNS data was shown to be substantially improved compared to that of the Bardina model, and an excessively high prediction of B-scatter in the Bardina model was substantially improved for both Reynolds numbers and both flows.

The validity of the F-Bardina model was established for two different flows and low/high Reynolds numbers. Further development of the present work is directed in two ways.

One is to investigate the correlation of the SGS energy production mechanism with the coherent vortical structures that resides in the turbulence. Preliminary results are reported in Horiuti (1995), but that study was conducted at the low Reynolds numbers. More refined and detailed examination of the high Reynolds number DNS data is necessary.

Another direction is to develop the SGS models based on the filtered-Bardina model. We must note that, although the F-Bardina model yielded very high correlation with the exact DNS data, its high correlation is decreased as the Reynolds number is increased as can be seen in Tables I-IV.

In fact, as the Reynolds number is increased, it is expected that the interscale interaction of GS with the distinctively smaller SGS will become significant as well as the interaction of GS with the larger SGS. An SGS model, which can be used to represent these two GS-SGS interactions, i.e., the local interaction between adjacent wave number bands and the nonlocal interaction between GS and very small

SGS, is desirable. The former interaction can be adequately represented using the F-Bardina model. In order to adequately represent the latter interaction, it is necessary to add the SGS EVM part to the model. That is, a mixed model of F-Bardina and Smagorinsky models is considered to be a more desirable and general model. A new dynamic two-parameter mixed model in which the two model parameters contained in the model were determined consistently with the dynamic SGS procedure (Germano *et al.* 1991) was proposed as an extension of the F-Bardina model (Horiuti 1996). Further refinement of the proposed model is currently underway.

Acknowledgments

I am grateful to the Center for Turbulence Research for its hospitality. Drs. N. N. Mansour and M. M. Rogers provided me with the DNS database. I am also grateful to Profs. P. Moin, and J. H. Ferziger for valuable discussions. This work was partially supported by the overseas research program, Ministry of Education, Science and Culture.

REFERENCES

Bardina, J. 1983 Improved turbulence models based on large eddy simulation of homogeneous, incompressible turbulent flows. *Ph.D. dissertation.* Stanford University, Stanford, California.

Durbin, P. A. 1993 A Reynolds stress model for near-wall turbulence. *J. Fluid Mech.* **249,** 465.

Germano, M., Piomelli, U., Moin, P. & Cabot, W. H. 1991 A dynamic subgrid-scale eddy viscosity model. *Phys. Fluids.* **A3,** 1760.

Ghosal, S., Lund, T. S., Moin, P. & Akselvoll, K. 1995 A dynamic localization model for large-eddy simulation of turbulent flows. *J. Fluid Mech.* **286,** 229.

Ghosal, S. & Moin, P. 1995 The basic equations for the large eddy simulation of turbulent flow in complex geometry. *J. Comp. Physics.* **118,** 24.

Härtel, C., Kleiser, L., Friedemann, U., & Friedrich, R. 1994 Subgrid-scale energy transfer in the near-wall region of turbulent flows. *Phys. Fluids.* **6,** 3130.

Horiuti, K. 1989 The role of the Bardina model in large eddy simulation of turbulent channel flow. *Phys. Fluids.* **A1,** 426.

Horiuti K. 1993a A proper velocity scale for modeling subgrid-scale eddy viscosity in large eddy simulation. *Phys. Fluids.* **A5,** 146.

Horiuti, K., Mansour, N. N., & Kim, J. 1993b A normal stress subgrid-scale eddy viscosity model in large eddy simulation. *Annual Research Briefs 1992* Center for Turbulence Research, NASA Ames/Stanford Univ., 61-71.

Horiuti, K. 1994 Assessment of the generalized normal stress and the Bardina Reynolds stress subgrid-scale models in large eddy simulation. *Direct and Large*

Eddy Simulation I, Ed. by P. R. Voke, L. Kleiser and J.-P. Chollet, Kluwer Acad. Pub., 85.

Horiuti, K. 1995 Subgrid-scale energy production mechanism in large eddy simulation. *Proc. of the International Symposium on Mathematical Modeling of Turbulent Flows,* Tokyo. 164.

Horiuti K. 1996 A new dynamic two-parameter mixed model for large-eddy simulation. Submitted to *Phys. Fluids.*

Horiuti, K. 1997 Backward scatter of subgrid-scale energy in wall-bounded and free shear turbulence. *J. Phys. Soc. Japan.* **66** (1).

Leslie, D. C. & Quarini, G. L. 1979 The application of turbulence theory to the formulation of subgrid modeling procedures. *J. Fluid Mech.* **91,** 65.

Mansour, N. N. 1996 Unpublished data.

Rogers, M. M. & Moser, R. D. 1994 Direct simulation of a self-similar turbulent mixing layer. *Phys. Fluids.* **6,** 903.

Piomelli, U., Zang, T. A., Speziale, C. G., & M. Y. Hussaini 1990 On the large-eddy simulation of transitional wall-bounded flows. *Phys. Fluids.* **A2,** 257.

Piomelli, U., Cabot, W. H., Moin, P. & Lee, S. 1991 Subgrid-scale backscatter in turbulent and transitional flows. *Phys. Fluids.* **A3,** 1766.

Smagorinsky, J. 1963 General circulation experiments with the primitive equations. I. The basic experiment. *Monthly Weather Review.* **91,** 99.

Speziale, C. G. 1985 Galilean invariance of subgrid-scale stress in large eddy simulation. *J. Fluid Mech.* **156,** 55.